International Journal of Mining Science and Technology 24 (2014) 549–558

Contents lists available at ScienceDirect

International Journal of Mining Science and Technology

journal homepage: www.elsevier.com/locate/ijmst

An improved method to assess the required strength of cemented backfill in underground stopes with an open face

Li Li *, Michel Aubertin

Department of Civil, Geological and Mining Engineering, École Polytechnique de Montréal, Montreal H3C 3A7, Canada

ARTICLE INFO

Article history:
Received 13 September 2013
Received in revised form 16 November 2013
Accepted 18 January 2014
Available online 6 June 2014

Keywords:
Underground mines
Backfill
Required strength
Analytical solutions
Numerical modeling
Mitchell's solution

ABSTRACT

Backfill is increasingly used in underground mines to reduce the surface impact from the wastes produced by the mining operations. But the main objectives of backfilling are to improve ground stability and reduce ore dilution. To this end, the backfill in a stope must possess a minimum strength to remain self-standing during mining of an adjacent stope. This required strength is often estimated using a solution proposed by Mitchell and co-workers, which was based on a limit equilibrium analysis of a wedge exposed by the open face. In this paper, three dimensional numerical simulations have been performed to assess the behavior of the wedge model. A new limit equilibrium solution is proposed, based on the backfill displacements obtained from the simulations. Comparisons are made between the proposed solution and experimental and numerical modeling results. Compared with the previous solution, a better agreement is obtained between the new solution and experimental results for the required cohesion and factor of safety. For large scale (field) conditions, the results also show that the required strength obtained from the proposed solution corresponds quite well to the simulated backfill response.

1. Introduction

Backfill is increasingly used in underground mines around the world. There are many environmental and economical benefits associated with underground backfilling for the mining industry [1,2]. Nonetheless, the primary objective of stopes backfilling is to provide a safe working space for miners and to increase mineral recovery by reducing ore dilution [3–6].

Many mines operate with primary and secondary stopes. The primary stopes are mined and then backfilled with a cemented fill, which must possess certain characteristics so that it can stand on its own during the mining of adjacent secondary stopes. The solution proposed by Mitchell et al. is commonly used to calculate the required strength for the cemented backfill in stopes with an open face [7]. A simple modification of this solution was proposed by Zou and Nadarajah, who took into account an overlying load (surcharge) [8]. Dirige et al. also proposed an analytical solution (inspired by, but distinct from that of Mitchell et al.) for estimating the required strength of backfill in stopes with inclined walls [7,9]. However, the latter may lead to an overly conservative design as it considers the hanging wall of the backfill as a free surface (without normal stresses); this assumption does not correspond to numerical modeling results, which show that non-negligible contact stresses may exist along the fill-hanging wall interface, depending upon the wall inclination, stope geometry and backfill properties [10]. The authors also proposed a modification of the Mitchell solution that is largely based on similar assumptions as those adopted by Mitchell et al.; the modified solution is typically (but not always) less conservative than the latter [7,11].

Mitchell et al. developed their original solution based on a limit equilibrium analysis [7]. To validate their solution, these authors conducted a series of box stability tests in the laboratory. These same test results will be used below to validate (in part) the solution proposed here, and to make a comparison with the original Mitchell solution.

In this paper, the solution proposed by Mitchell et al. is first recalled [7]. Some of the main assumptions behind the underlying wedge model are examined. Three dimensional numerical simulations are then presented to assess the mechanical response of the backfill upon exposure due to removal of a vertical (supporting) wall. A new analytical solution is proposed for the exposed backfill strength, taking into account the simulation results regarding the displacement and apparent failure mechanism. This improved solution is compared with experimental data for validation purposes.

* Corresponding author. Tel.: +1 514 340 4711.
E-mail address: li.li@polymtl.ca (L. Li).

http://dx.doi.org/10.1016/j.ijmst.2014.05.020
2095-2686/

2. Wedge block model

2.1. Original solution

Fig. 1 shows the wedge block model used by Mitchell et al. to develop an analytical solution for estimating the factor of safety (*FS*) of a stope upon exposure of the unsupported backfill [7]. The corresponding values of *FS* can be formulated as:

$$FS = \frac{\tan\phi}{\tan\alpha} + \frac{2cL}{H^*(\gamma L - 2c_b)\sin 2\alpha} \tag{1}$$

where B and L are the stope length and width, respectively; α the assumed angle between the sliding and horizontal planes at the base of the wedge; c and ϕ the cohesion and internal friction angle of the backfill (based on the Coulomb failure criterion), respectively; c_b the bond cohesion (adherence) along the interface between the side walls and backfill; and H^* ($=H-(B\tan\alpha)/2$, where H is the actual height) is an equivalent height of the wedge block.

Assuming $c_b = c$, Eq. (1) can be used to evaluate the required backfill strength (cohesion); this leads to the following equation:

$$2c = \frac{(FS - \frac{\tan\phi}{\tan\alpha})\gamma H^* L \sin 2\alpha}{(FS - \frac{\tan\phi}{\tan\alpha})H^* \sin 2\alpha + L} \tag{2a}$$

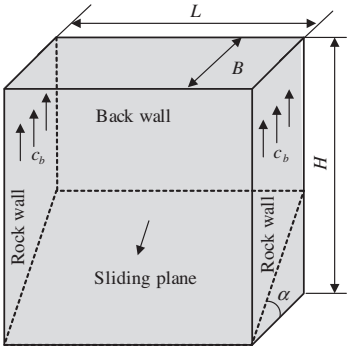

Fig. 1. Wedge block model [7].

By further considering $H \gg B$ (thus $H^* \approx H$), Mitchell et al. expressed the required backfill cohesion as follows (for $FS = 1$) [7]:

$$c = \frac{\gamma H}{2(H/L + \tan\alpha)} \tag{2b}$$

where the sliding plane angle α is dependent on the fill friction angle ϕ (i.e. $\alpha = 45° + \phi/2$, for the commonly used assumption).

For the specific case (considered by Mitchell et al. [7]) where $\phi = 0$ (or $\alpha = 45°$), $c_b = c$, and $H \gg B$, Eq. (1) reduces to the following:

$$FS = \frac{2cL}{H(\gamma L - 2c)} \tag{3}$$

The required unconfined compressive strength, UCS ($=2c$, for $\phi = 0$) can then be expressed from Eq. (2b) or Eq. (3) as follows (for $FS = 1$):

$$UCS = 2c = \frac{\gamma H}{1 + H/L} \tag{4}$$

Eq. (4) was proposed by Mitchell et al. to define the minimum strength of cemented backfills in stopes with an unsupported (open) face [7].

To validate this solution (Eq. (4)), Mitchell et al. performed a series of box stability tests conducted using a laboratory physical model [7]. Their main experimental results are summarized in Table 1. Fig. 2 shows a comparison of the required cohesion obtained from the experimental and predicted results. These tend to indicate that this solution often overestimates the required strength of the backfill, especially for stopes having a relatively low (height to length) aspect ratio ($H/L < 3.5$), leading to uneconomic design. The relatively poor correlation between this solution and the experimental results is further illustrated in Fig. 3 in terms of *FS*; this figure indicates that the analytical solution often tends to underestimate the factor of safety (i.e. $FS < 1$), particularly in the case of low (height to length) aspect ratio openings.

The Mitchell et al. solution presented above was developed based on following hypotheses [7]:

(i) The potential sliding surface near the base of the stope makes an angle α with the horizontal, which is assumed to be $\alpha = 45° + \phi/2$ (corresponding to the Rankine active case).

Table 1
Physical model test results of backfilled stopes after removal of the front wall [7].

Test No.	L (m)	B (m)	H (m)	γ (kN/m[c])	α (°)	Average direct shear strength, c_b (kPa)		
						Samples[a]	Control[b]	Corrected[c]
S13	0.8	0.2	0.8	19.5	68	3.1	3.00	3.30
S15	0.8	0.2	0.8	19.4	69	2.9	3.40	3.40
S7	0.8	0.4	0.9	19.7	60	2.7	2.70	2.70
T10	0.8	0.4	0.9	18.7	63	2.8	3.00	3.00
S14	0.8	0.2	1.0	19.3	66	4.0	4.00	4.00
S18	0.6	0.2	0.8	19.4	66	3.2	3.20	3.20
S16	0.6	0.2	0.8	19.3	70	2.7	3.00	3.00
S4	0.4	0.2	0.6	19.7	60	2.2	2.00	2.20
S17	0.6	0.2	0.9	19.6	56	2.5	3.25	3.00
S8	0.8	0.4	1.3	18.8	60	3.8	3.50	4.00
T9	0.8	0.4	1.4	19.0	72	3.0	3.50	3.50
T11	0.8	0.4	1.6	18.9	65	4.2	5.00	4.40
T6[d]	0.8	0.4	1.8	19.5	62	4.4	n.a.	4.90
T12[d]	0.8	0.2	1.8	18.9	65	4.0	n.a.	4.50
S27	0.6	0.2	1.5	18.3	78	3.5	3.50	3.60
S28	0.6	0.2	1.5	18.1	66	3.6	3.75	3.85
S20	0.6	0.4	1.8	18.5	60	3.4	3.50	3.60
S1A	0.4	0.2	1.4	20.0	61	3.2	3.10	3.20

[a] Measured values from direct shear tests done on samples taken from either the intact parts of a failed block or from the material left in the formwork after each test was completed.
[b] Measured values from control direct shear tests, carried out just before fill exposure.
[c] Back calculated values based on the average normal stress on the observed sliding surface for each failure [7].
[d] Failure with a surcharge of 450 N (45 kg in mass).

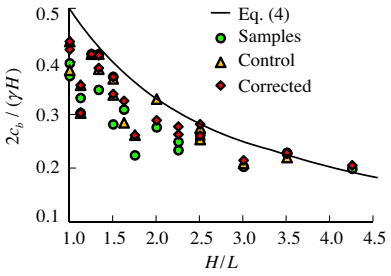

Fig. 2. Comparison between experimental results and predicted values obtained from Eq. (4) ("Samples" and "Control" mean strength parameters obtained with direct shear tests while "Corrected" means back calculated strengths, see Table 1 for more details).

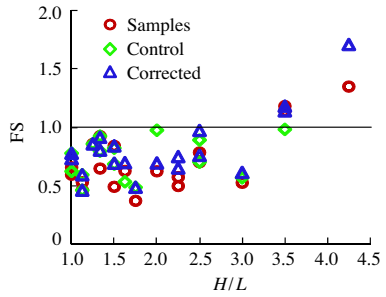

Fig. 3. Factor of safety (*FS*) calculated with the solution proposed by Mitchell et al. (Eq. (4)) for the box stability experimental tests [7].

(ii) The friction angle of the backfill on the sliding plane can be neglected, i.e. $\phi \approx 0$, leading to $\alpha = 45° + \phi/2$ (and $UCS = 2c$, as seen above).
(iii) The wedge block is submitted to shearing stresses along the interfaces between the backfill and the two lateral rock walls:
  a) These shear stresses are due to bond cohesion (adherence) only, with $c_b = c$ (and $\delta = 0$);
  b) The shear stresses along the lateral walls were assumed to act along the vertical upward direction (Fig. 1).
(iv) There is no shear and normal stresses between the sliding block and the back wall (opposite to the exposed face).
(v) The stope is narrow and high, with $H \geqslant B \tan\alpha$, so that the sliding plane intersects the back wall.
(vi) There is no surcharge applied on top of the backfill (n.a.: a surcharge was nonetheless applied in some of the experimental tests; see T6 and T12 in Table 1).

In the following, these hypotheses will be examined using numerical modeling results and laboratory testing data.

2.2. Shear stresses in backfill and along fill-rock interfaces

In the solution proposed by Mitchell et al., the shear strength due to friction is neglected for the backfill and along the fill-rock interfaces [7]. Thus, the internal friction angle of the backfill, ϕ, and the friction angle along the fill-wall interfaces, δ, were taken as zero. Only cohesion is taken into account. The justification for this assumption is that the cement bond strength is mobilized under both small and large stresses, while the frictional resistance is only developed at relatively large strains. This "broken before shearing" approach was based on some shear box and unconfined compression tests results, but details of these tests were not given. It is however difficult to understand why effective stresses, under fully drained condition (no excess pore water pressure), would not contribute to the shear strength of the backfill material in stopes upon removal of the wall. This questionable assumption may have been related to the small stresses induced in the physical models, which render the magnitude of this frictional strength (almost) insignificant. But this hypothesis is not compatible with their unconfined compression tests results which showed rupture planes making angles varying from 50° to 65° to the major principal plane, indicating a friction angle varying from 10° to 40° (for the commonly used assumption $\alpha = 45° + \phi/2$) [7,12]. Observations made during their box stability tests showed sliding planes making angles varying from 56° to 78° to the horizontal (see Table 1), indicating a fill friction angle of at least 22°. These results tend to indicate that the tested cemented backfills typically have a frictional strength component, under drained conditions (as other geomaterials). Hence, hypothesis (ii) ($\phi = 0$) adopted by Mitchell et al. seems unjustified here [7].

Regarding the strength of fill-wall interface, it is a common practice in geotechnical engineering to assume $\delta = \phi_{mob} < \phi_{peak}$ along interfaces (ϕ_{mob} and ϕ_{peak} are the mobilized and peak friction angles of the backfill, respectively [13]). In practice, an effective friction angle equal to two third of the internal friction angle, i.e., $\delta = (2\phi)/3$, is often used [14,15].

Recently, Fall and Nasir conducted a series of laboratory tests to study the mechanical properties of interface between cemented paste backfill (CPB) and rough surfaces made from bricks, and concrete [16]. Their results showed that the ratio between the CPB's cohesion, c, and the adherence along the interfaces, c_b, becomes very small after 28 days of curing ($c_b/c < 0.1$). The difference was much less significant for the friction angle between the CPB and interfaces, i.e. $\delta \approx \phi$. These results suggest that the two corresponding hypotheses ((ii) and (iii)-a) in the model proposed by Mitchell et al. may not be representative of backfill behavior along the interfaces [7].

The solution of Mitchell et al. also neglects the shear resistance along the interface between the backfill and back wall, but this assumption can also be questioned [7]. The relatively small size and low stress magnitude for the box tests (compared to in situ values) may have contributed to this apparent lack of strength along the back wall (which may have been too small to be of significance in this case). This assumption would not be representative of the ground conditions in the field, where some contact should remain between the backfill and (vertical) back wall even when the front wall is removed (based in part on the simulations results shown below). Consequently, it is inferred here that hypothesis (iv) adopted by Mitchell et al. is not representative of the actual conditions [7].

2.3. Numerical simulations of backfilled stopes with an open face

Numerical simulations have been performed using the commercial software FLAC3D to investigate the response of backfill, based on an elasto-plastic approach [17]. Fig. 4 shows half of a high and narrow stope model (plane symmetry is considered) with $H = 40$ m, $L = 8$ m, and $B = 10$ m. The backfill properties are as follows (based on the Mohr–Coulomb elasto-plastic model):

$E_b = 300$ MPa (Young's modulus), $\mu_b = 0.3$ (Poisson's ratio), $\phi_b = 30°$ (friction angle), $\psi = 0°$ (dilation angle), $\gamma_b = 18$ kN/m^3 (dry unit weight).

The rock mass is considered linear elastic, with the following properties:

$E_r = 30$ GPa (Young's modulus), $\mu_r = 0.25$ (Poisson's ratio), $\gamma_r = 27$ kN/m^3 (unit weight).

The numerical modeling sequence involves the creation of the stope first. The fill is then placed in the stope in 8 layers, after the release of the elastic deformation in the rock. Once filling is

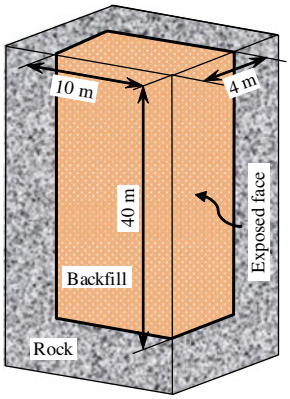

Fig. 4. FLAC3D model representing half of a high and narrow stope (plane symmetry is considered) with H = 40 m, L = 8 m, and B = 10 m.

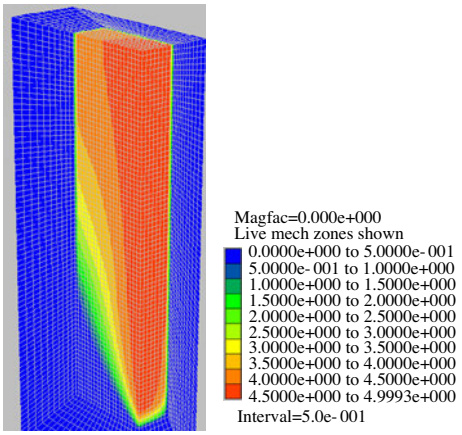

Fig. 5. Distribution of displacement of the backfill simulated with FLAC3D for the high and narrow stope with an open face with c = 0.

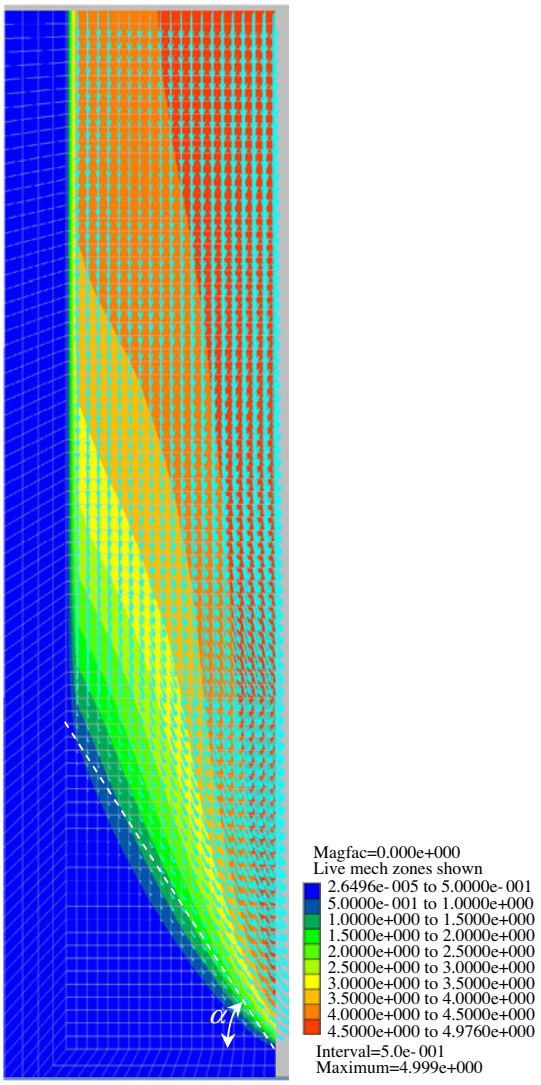

Fig. 6. Displacement distribution and corresponding vectors toward the open face (right hand side) obtained with FLAC3D for the high narrow backfilled stope with c = 0.

complete (up to 40 m), a cohesion value (if applicable) is given to the fill to simulate the gain of strength due to the binder.

Fig. 5 presents a three dimensional view of the backfill displacement after the removal of the front wall. The simulation is performed by considering small strain (to limit numerical instability). It can be seen that a block that has a shape quite similar to the wedge model of Mitchell et al., but with a slightly curved surface at the base, appears in this view [7]. Examination of the "sliding" plane indicates that it makes an angle of about $\alpha \approx 51°$ to the horizontal (Fig. 6). This value is somewhat lower than the value of 60° given by the commonly used relationship (i.e. $\alpha = 45° + 30°/2 = 60°$).

Fig. 6 also reveals that the movement of the sliding block can be divided into two zones. The zone above the base triangle (called the upper zone) mainly moves downward (in the vertical direction), while the triangular zone (lower zone) moves down and toward the opening in a direction quasi-parallel to the sliding plane. This indicates that the shear resistance of the lower zone along the interfaces between side walls and backfill acts in a direction parallel to the sliding plane at the base. This sliding mechanism does not correspond well to the hypothesis (iii)-b of Mitchell et al., who considered that the shear resistance along the two side walls acts in the vertical direction [7].

3. Proposed solution

3.1. New formulation

Based on the numerical analyses presented above and on recent experimental observations, the following assumptions are adopted to develop a new formulation for the stress state in narrow backfilled stopes with an unsupported face (Fig. 7) [16,18–20]:

(i) The stope is high and narrow, i.e. $H \geqslant B \tan\alpha$.
(ii) The sliding surface makes an angle $\alpha = 45° + \phi'/2$ with the horizontal.
(iii) The moving block consists of two parts: the upper rectangular block and the lower triangular wedge.
(iv) The shear resistance along the interface between the upper block and the back wall acts in the upward vertical direction. The shear resistance due to friction along this wall is neglected, as the normal stresses along the back wall are

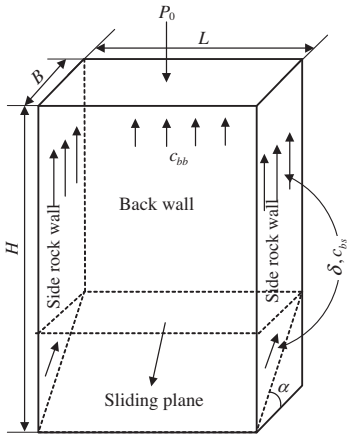

Fig. 7. New confined block model of a high and narrow stope.

expected to be low once the front wall is removed. The interface cohesion (adherence), c_{bb}, along this wall is proportional to the backfill cohesion, c:

$$c_{bb} = r_{bb}c \tag{5a}$$

where r_{bb} is a parameter that controls the interface cohesion along the back wall ($0 \leqslant r_{bb} \leqslant 1$).

(v) Both cohesion (c_{bs}) and friction (δ) contribute to the shear resistance along the side walls of the two blocks. The resulting stresses act in the vertical direction along the interfaces between the upper block and the side walls, and in a direction parallel to the sliding plane along the interfaces between the lower wedge of backfill and the side walls. The interface cohesion (adherence), c_{bs}, between the backfill and the side walls is also expressed as a ratio of the backfill cohesion, c:

$$c_{bs} = r_{bs}c \tag{5b}$$

where r_{bs} is a parameter for the interface cohesion between the backfill and the side walls ($0 \leqslant r_{bs} \leqslant 1$).

(vi) A surcharge, P_0, can be applied on top of the backfill (which may be due for instance to additional fill material or to equipment).

Fig. 8 shows the decomposition of the sliding block (Fig. 7) into the upper rectangular block (left side) and lower triangular wedge (right side), with the acting forces. The upper block is submitted to a surcharge P_0 ($=p_0 \times B \times L$; p_0 is the corresponding pressure due to the surcharge), normal (N_1) and shear (S_1) forces along the interfaces between the backfill and side walls, shear force (S_2) along the interface between the backfill and back wall, and the weight of the block, W_1. The lower wedge is submitted to normal (N_0) and shear (S_0) forces along the inclined sliding plane, normal (N_3) and shear (S_3) forces along the interfaces between the backfill and two side walls, and the weight of the wedge, W_0. The force P_1 ($=p_1 \times B \times L$; p_1 is the corresponding pressure at the boundary between the upper and lower blocks), which supports the base of the upper block, constitutes a surcharge for the lower wedge.

The weight of the upper block is obtained as follows:

$$W_1 = \gamma BL(H - H') \tag{6}$$

with

$$H' = B\tan\alpha \tag{7}$$

The force components N_1, S_1, and S_2, can be obtained from the stresses in the backfilled stope. These are expressed as follows for a given depth h [21,22]:

$$\sigma_{hh} = K\left\{\frac{\gamma}{M}[1 - \exp(-hM)] + p_0\exp(-hM)\right\} \tag{8}$$

where parameter M is expressed as:

$$M = 2K(B^{-1} + L^{-1})tan\delta \tag{9}$$

In the above equations, K is an earth pressure coefficient. The authors' previous investigations indicate that the value of K in vertical stopes is typically close to Rankine's active earth pressure coefficient, i.e. $K = K_a = \tan^2(45° - \phi/2)$ [21–25].

The two exponential terms on the right had side of Eq. (8) are related to the arching effect, which tends to reduce the stresses at depth due to a transfer to the rigid walls [10,11,21–25].

The normal force N_1 can then be estimated as follows:

$$N_1 = \int_0^{H-H'} \sigma_{hh} B dh = \frac{KB}{M}\left\{\gamma(H - H') + (p_0 - \frac{\gamma}{M})[1 - \exp(-(H - H')M)]\right\} \tag{10}$$

Shear resistances S_1 and S_2 can then be obtained by considering that the (Coulomb) shear strength is fully mobilized along the interfaces between the backfill and the three walls:

$$S_1 = c_{bs}B(H - H') + N_1\tan\delta \tag{11a}$$

$$S_2 = c_{bb}L(H - H') \tag{11b}$$

Considering the equilibrium of the upper block, the pressure, p_1 ($=P_1/(B \times L)$) acting at the base of the upper block can be expressed as follows:

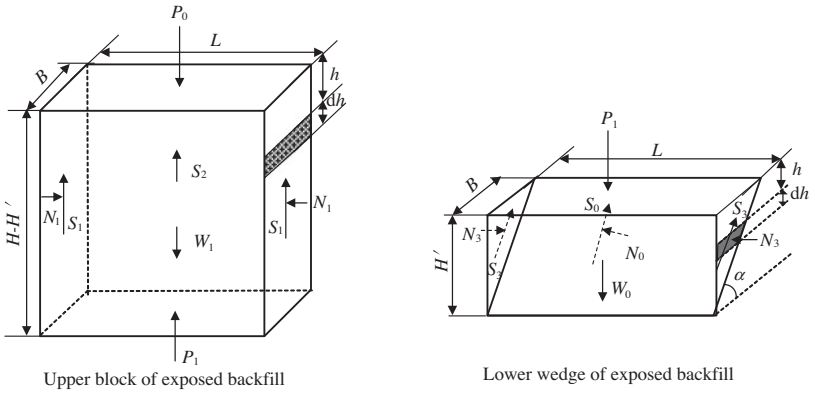

Fig. 8. Decomposition of the forces acting on the two components of the block model.

$$p_1 = p_0 + \frac{W_1 - 2S_1 - S_2}{BL} \tag{12}$$

Replacing the relevant terms by their corresponding equations gives:

$$p_1 = p_0 - G' + (H - H')\left\{\gamma - c\left(\frac{2r_{bs}}{L} + \frac{r_{bb}}{B}\right)\right\} \tag{13}$$

where parameter G' is expressed as:

$$G' = \frac{1}{1 + L/B}\left\{\gamma(H - H') + \left(p_0 - \frac{\gamma}{M}\right)[1 - \exp(-(H - H')M)]\right\} \tag{14}$$

As a special case, if $\delta = 0$, $M \to 0$, Eq. (13) reduces to following equation:

$$p_1 = p_0 + (H - H')\left\{\gamma - c\left(\frac{2r_{bs}}{L} + \frac{r_{bb}}{B}\right)\right\} \tag{15}$$

It is seen that the arching effect (exponential term) disappears for this latter condition.

The weight of the lower triangle wedge, W_0, is given as:

$$W_0 = \frac{1}{2}\gamma BLH' = \frac{\gamma LH'^2}{2\tan\alpha} \tag{16}$$

Using the arching solution proposed by the authors, the normal force N_3 is expressed as follows [21,22]:

$$N_3 = \int_0^{H'} \sigma_{hh} B\left(1 - \frac{h}{H'}\right)dh = \frac{K}{M\tan\alpha}\left\{\left(\frac{\gamma}{M} - p_1\right)\left(\frac{1 - \exp(-H'M)}{M} - H'\right) + \frac{\gamma H'^2}{2}\right\} \tag{17}$$

The shear resistance S_3 is obtained by considering a fully mobilized (Coulomb) shear strength along the interfaces between the backfill and the side walls:

$$S_3 = c_{bs}\frac{H'^2}{2\tan\alpha} + N_3\tan\delta \tag{18}$$

The equilibrium of the triangular wedge in the direction normal to the sliding plane leads to:

$$N_0 = (p_1 BL + W_0)\cos\alpha \tag{19}$$

The shear resistance S_0 is also obtained from the fully mobilized shear strength along the sliding plane:

$$S_0 = c\frac{H'L}{\sin\alpha} + N_0\tan\phi \tag{20}$$

The equilibrium of the wedge then gives the factor of safety, FS, against sliding along the inclined plane:

$$FS = \frac{S_0 + 2S_3}{(p_1 BL + W_0)\sin\alpha} \tag{21}$$

Replacing the relevant terms by their corresponding expression, the following equation is obtained for the value of FS against sliding along the inclined plane:

$$FS = \frac{\tan\phi}{\tan\alpha} + \frac{c\left(\frac{1}{\cos\alpha} + r_{bs}\frac{H'}{L}\right) + \frac{(\gamma/M - p_1)[(1 - \exp(-MH'))/(MH') - 1] + \gamma H'/2}{1 + L/B}}{(p_1 + \gamma H'/2)\sin\alpha} \tag{22}$$

The required cohesion can then be deduced from Eq. (22):

$$c = \frac{D'(p_0 + \gamma(H - H') - G') + \frac{A'\gamma H'}{2}\left(1 + \frac{L}{B}\right)\sin\alpha - \gamma\left(\frac{C'}{M} + \frac{H'}{2}\right)}{B'\left(1 + \frac{L}{B}\right) + D'(H - H')\left(\frac{2r_{bs}}{L} + \frac{r_{bb}}{B}\right)} \tag{23}$$

where

$$A' = FS - \frac{\tan\phi}{\tan\alpha} \tag{24}$$

$$B' = \frac{1}{\cos\alpha} + r_{bs}\frac{H'}{L} \tag{25}$$

$$C' = \frac{1 - \exp(-MH')}{MH'} - 1 \tag{26}$$

$$D' = A'\left(1 + \frac{L}{B}\right)\sin\alpha + C' \tag{27}$$

The use of this new analytical solution (Eqs. (22) and (23)) is illustrated with a few sample calculations given in Li and Aubertin [26].

3.2. Graphical representation

Fig. 9 shows the variation of the factor of safety FS with an increase of the backfill cohesion c (according to Eq. (22)) for an adherence coefficient r_b (considered identical for the side and back walls, i.e., $r_b = r_{bb} = r_{bs}$) that varies from 0 to 1, for a frictionless condition along the walls ($\delta = 0$; Fig. 9a) and with fully frictional interfaces along the side walls ($\delta = \phi$; Fig. 9b). The results indicate that the factor of safety tends to increase only slightly, and almost linearly, with the backfill cohesion, c, when $r_b \approx 0$ (no adherence). When the interfaces cohesion ($c_{bb} = c_{bs}$) is close to that of the backfill (i.e. $r_b = 1$), the factor of safety increases much more significantly with the latter. The intermediate situation with $c_{bb} = -c_{bc} = 0.5c$ indicates a lesser effect of cohesion on the value of FS. These results also indicate that the backfill stability can be significantly improved when friction is mobilized along the interfaces (Fig. 9b compared with frictionless interfaces, Fig. 9a). Rougher walls may thus be beneficial in this regard.

Fig. 10 presents the factor of safety (Fig. 10a) and the required backfill strength (Fig. 10b) as a function of the adherence coefficient, r_b, obtained from Eqs. (22) and (23), when the interface friction angle δ increases from 0 to ϕ. It is observed that the stability of the exposed backfill block increases nonlinearly with the adherence coefficient, r_b (Fig. 10a). The required backfill cohesion then tends to decrease, in a nonlinear manner, with this adherence coefficient, r_b (Fig. 10b). These graphs also indicate that an increase in the backfill-wall friction angle, δ, improves the stability of the exposed backfill (Fig. 10a), while decreasing the required backfilled cohesion (Fig. 10b). Again, this behavior can be favored by rougher walls in stopes.

Fig. 11 illustrates the variation of the factor of safety (Fig. 11a) and of the required strength (Fig. 11b) as a function of the adherence coefficient, r_b, obtained from Eqs. (22) and (23), when the backfill friction angle ϕ increases from 20° to 40°. These follow similar tendencies as those observed in Fig. 10, indicating that the backfill stability is improved, or the required backfill cohesion is decreased, when there is an increase of the backfill friction angle, ϕ, or/and of the fill-wall interface adherence, r_b.

Fig. 12 shows the variation of FS (Fig. 12a) and of the required cohesion c (Fig. 12b) with an increase of backfill height, H, for different adherence coefficient, r_b. As expected, the stability of the backfill decreases with an increase of stope height, H (Fig. 12) for a given cohesion, c. The required backfill cohesion, c, thus increases for higher stopes (Fig. 12b), particularly when the interface adherence is low ($r_b \leqslant 0.5$). However, it is worth noting that the values of FS and required backfill cohesion tend to become constant when the stope height exceeds about 28 m for $r_b = 1$.

Fig. 13 presents the variation of FS (Fig. 13a) and of the required cohesion c (Fig. 13b) with an increase of stope width, L, for different cohesion coefficient, r_b. As expected, the backfill stability decreases significantly with wider stope, while the required backfill cohesion increases markedly. This suggests that narrow primary stopes should be favored in backfilling schemes to improve stability. The values of FS and required backfill cohesion tend toward a constant when the stope width exceeds certain size. This seems due to the fact that the stabilization effect provided by fill-side wall shear strength is reduced with wider stope. When the

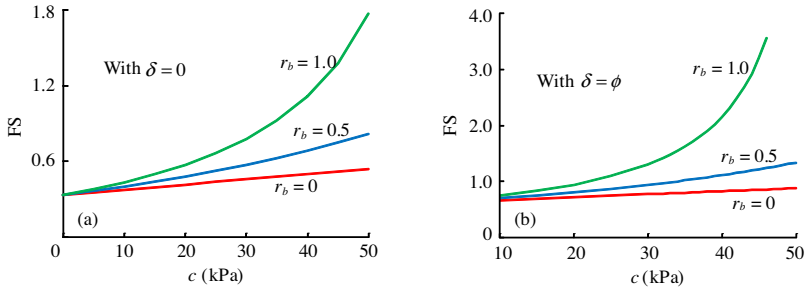

Fig. 9. Variation of *FS* with the backfill cohesion *c* for the cases of (a) low friction and (b) large friction along the walls (the calculations have been done for H = 40 m, B = 10 m, L = 8 m, γ = 18 kN/m^3, ϕ = 30°, and p_0 = 0).

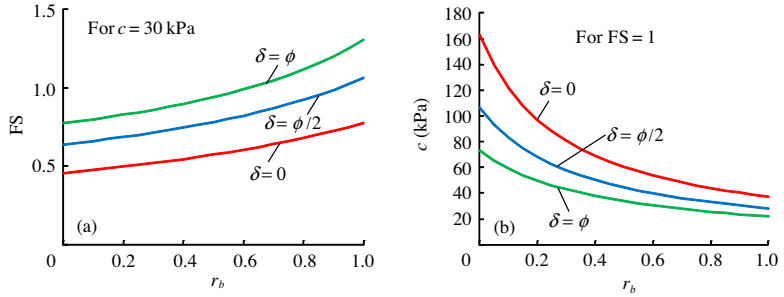

Fig. 10. Variation of the (a) *FS* (for c = 30 kPa) and (b) required cohesion c (for *FS* = 1) with the adherence coefficient r_b for different friction angles between the backfill and the side walls, δ (the calculations have been made for H = 40 m, B = 10 m, L = 8 m, γ = 18 kN/m^3, ϕ = 30°, and p_0 = 0).

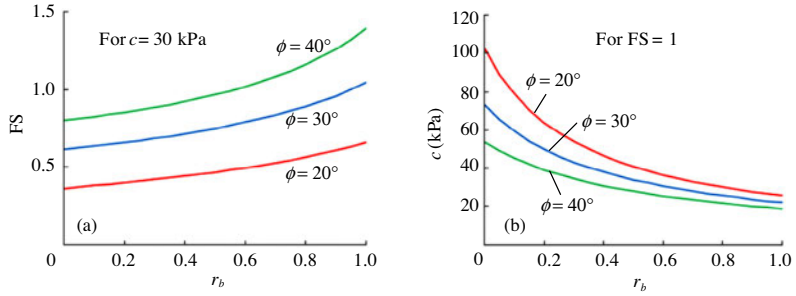

Fig. 11. Variation of the (a) *FS* (for c = 30 kPa) and (b) required cohesion c (for *FS* = 1) with the adherence coefficient r_b for different friction angles, ϕ (the calculations have been made for H = 40 m, B = 10 m, L = 8 m, γ = 18 kN/m^3, $\delta = \phi$, and p_0 = 0).

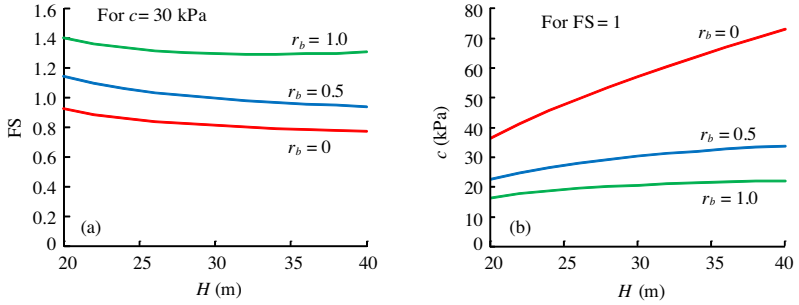

Fig. 12. Variation of the (a) *FS* (for c = 30 kPa) and (b) required cohesion c (for *FS* = 1) with the stope height, H, for different adherence coefficients, r_b (the calculations have been made for B = 10 m, L = 8 m, γ = 18 kN/m^3, $\delta = \phi$ = 30°, and p_0 = 0).

stope is wide enough, the influence of the two side walls can be neglected and the problem can be treated as two dimensional.

Fig. 14 illustrates the variation of *FS* (Fig. 14a) and of the required cohesion c (Fig. 14b) with an increase of stope length, B, for different adherence coefficient, r_b. As this adherence cohesion is the only source of shear strength along the back wall, the contribution from this shear strength when r_b is small ($\leqslant$0.5 in this case) can become negligible compared with the strength mobilized along the side walls. With a longer stope, the contact area between the backfill and the side walls becomes larger, leading to an

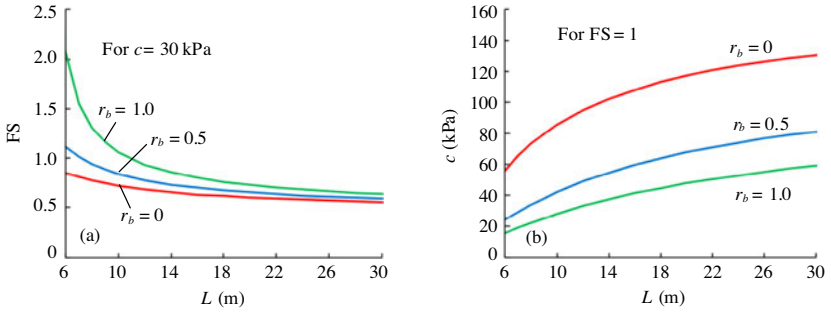

Fig. 13. Variation of the (a) *FS* (for $c = 30$ kPa) and (b) required cohesion c (for $FS = 1$) with the stope width, L, for different adherence coefficients, r_b (the calculations have been made for $H = 40$ m, $B = 10$ m, $\gamma = 18$ kN/m^3, $\delta = \phi = 30°$, and $p_0 = 0$).

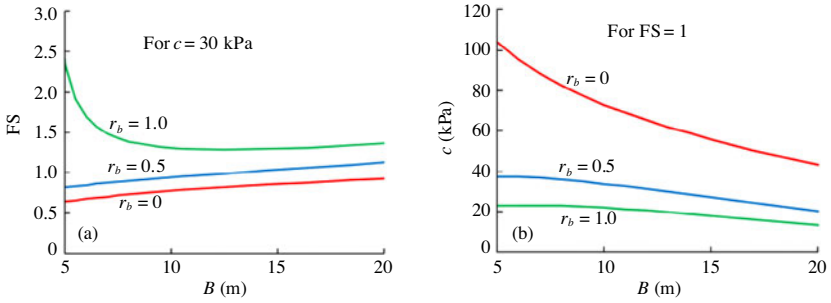

Fig. 14. Variation of the (a) *FS* (for $c = 30$ kPa) and (b) required cohesion c (for $FS = 1$) with an increase of stope length, B for different cohesion coefficients r_b (the calculations have been made for $H = 40$ m, $L = 8$ m, $\gamma = 18$ kN/m^3, $\delta = \phi = 30°$, and $p_0 = 0$).

improved backfill stability and a reduction in the required cohesion. When the interface adherence is high (r_b near 1), the backfill stability depends on the combined effects of the strength along the side wall and back walls. In this case, an increase of stope length B leads to an increase of contact area along the side walls, but to a reduction of the contact area along the back wall. The results show that the backfill stability decreases when B is increased up to a maximum value ($B = 12.5$ m in this case); thereafter, *FS* tends to increase with the stope length, B. Nonetheless, for given set of conditions (parameters), the factor of safety obtained with $r_b = 1.0$ is always higher and the required cohesion is always lower than when $r_b \leqslant 0.5$. These results indicate that longer stopes can be advantageous in terms of backfill stability and required strength; this may help reduce cement consumption.

3.3. Comparisons with experimental results

As mentioned above, Mitchell et al. performed a series of experimental tests, using cemented tailings and sands, within a box of $2.0 \times 1.8 \times 0.9$ m [7]. The main testing results have been presented in Table 1, which gives only the successful backfill failure tests. Comparing these tests results with the solution proposed here requires that the values of parameters ϕ, δ, c_{bb} and c_{bs} be known. Analyses have been conducted to determine the optimal values for these parameters (which have not been measured directly) based on the minimization of the following error function:

$$Err = \sqrt{\sum \left(c_{\text{calculated}} - c_{\text{measured}}\right)^2}$$

where $c_{\text{calculated}}$ and c_{measured} are the required cohesion calculated with the proposed solution (Eq. (23)) and the measured cohesion, respectively.

The optimal solution for all the tests gives $\delta = \phi = 17.05°$, $r_b = 26.87\%$ and $Err = 1.548$. This solution was obtained by applying a curve fitting technique with the predefined condition $\delta \leqslant \phi$.

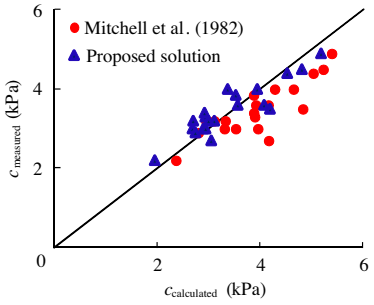

Fig. 15. Measured cohesion versus required cohesion calculated with the solution of Mitchell et al. (circle) and the proposed solution (triangle) using parameters $\delta = \phi = 17.05°$, $r_b = 26.87\%$ [7].

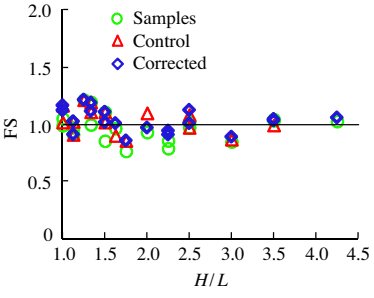

Fig. 16. *FS* for the box stability tests performed by Mitchell et al. calculated with the proposed solution (Eq. (22)) using $\delta = \phi = 17.05°$, $r_b = 26.87\%$; the "Samples", "Control" and "Corrected" data are given in Table 1 [7].

Fig. 15 shows a comparison between the measured cohesion and the required cohesion estimated with the proposed solution using these parameters. The figure also shows, as a general indicator, the required cohesion calculated with the solution of Mitchell et al. [7].

These results indicate that the improved solution proposed here correlates well with the experimental data.

Fig. 16 shows the values of *FS* for the box stability tests performed by Mitchell et al., calculated with the proposed solution (Eq. (22)) using the above mentioned parameters [7]. When compared with the results shown in Fig. 3, Fig. 16 shows that the proposed solution leads to improved estimates of *FS*, which are expected to be close to unity at the onset of failure during the box stability tests.

It should be recalled here, however, that these physical model tests were conducted at a scale that is much smaller than the in situ conditions (leading to much smaller stresses), while some other characteristics were not representative of actual ground conditions in the field. Hence, these experimental results constitute only a partial indication of the validity of the proposed solution (or of any other solution).

3.4. Numerical simulations to evaluate the required strength

To help with the evaluation of the proposed solution with more representative conditions in terms of stope geometry, additional simulations have been conducted with FLAC3D to assess some of the characteristics of the backfilled stopes upon the front wall removal. Fig. 17 shows the backfill displacement distribution after the removal of the front wall when the backfill cohesion varies from 0 to 30 kPa, using the same geometry and material properties as in the simulation shown in Fig. 4. Except for case (a) where a small strain condition was used in the simulation to achieve numerical convergence, the other calculations were performed with the large strain option to have a better view of the mesh deformation after the removal of the front wall. These numerical simulations were performed without interface elements between the backfill and the rock walls; this corresponds to a condition with $\delta = \phi$ (=30°) and $c = c_b$ (i.e. $r_b = r_{bs} = r_{bb} = 1$). These figures indicate that the backfill is unstable when cohesion $c \leqslant 20$ kPa (with a maximum displacement of 5.6 m), while it is stable when c reaches 30 kPa (with a maximum displacement of 3.2 cm), suggesting that the critical cohesion value is between 20 and 30 kPa in this situation. For this case, the proposed solution (Eq. (23)) gives $c = 22.04$ kPa for the required backfill cohesion (Li and Aubertin), while the solution of Mitchell et al. leads to a value of 72 kPa (with Eq. (4)) [7,26]. This suggests again that the Mitchell et al. solution tends to overestimate significantly the required strength, leading to non economical design in some instances [7]. The solution proposed here appears more realistic, based on this analysis.

4. Final remarks

The interaction between backfill and adjacent rock mass can be quite complex, especially when one of the supporting walls is removed. Simplifying assumptions have to be adopted to develop analytical solutions for this situation. As limited numerical modeling and experimental results are available, it is not straightforward to select the most appropriate hypotheses in terms of geometry and material properties. More elaborated testing programs are desirable in order to obtain additional results to validate such assumptions.

A wedge model composed of an upper rectangular block and a lower triangular wedge was considered here. The former was assumed to move along the vertical direction while the latter moves in a direction parallel to the sliding plane; the internal shear stress that could be generated between these two blocks was neglected. This aspect needs to be further investigated to assess the validity of this assumption.

Another limitation of the approach used here is related to the stress distribution in backfilled stopes, which has been based on the one proposed by the authors [21,22]. As this solution simplifies

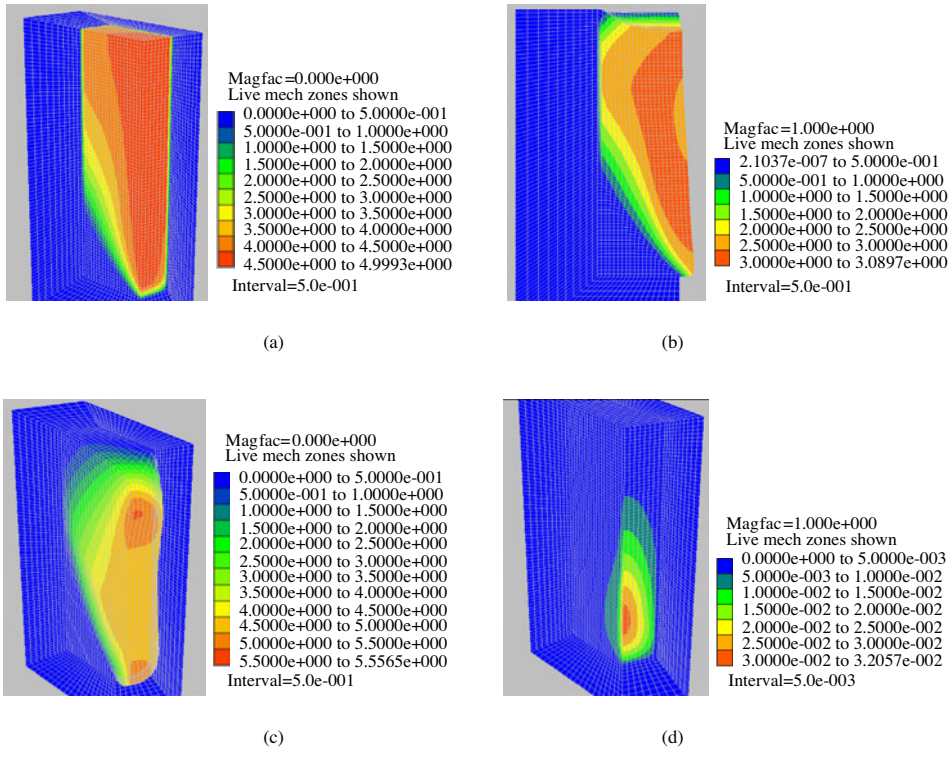

Fig. 17. Simulated backfill displacement (in meter) distribution after the removal of the front wall when the backfill cohesion varies from 0 to 30 kPa: (a) $c = 0$ kPa (failure); (b) $c = 10$ kPa (failure); (c) $c = 20$ kPa (failure); (d) $c = 30$ kPa (stable) (the characteristics of the model are given in Fig. 6).

the effect of removing the front wall, additional work is thus required to validate this stress estimate.

Other aspects that should be taken into account to further improve the solution include the effect of the backfill dilation angle, introduction of a more representative constitutive model, the potential impact of the fill desiccation near the surface, and the influence of wall inclination and stope size (which affect the magnitude and orientation of the stresses). These issues are part of the ongoing work performed by the authors and coworkers.

5. Conclusions

In this paper, the commonly used solution proposed by Mitchell et al. for the design of backfilled stope with an open face is reviewed [7]. Based on observations of backfill behavior obtained from laboratory tests on physical models and numerical modeling, a new analytical solution is proposed, in which the mobilized shear strength involves both friction and cohesion along the potential sliding planes, including the interfaces between the backfill and rock walls. Comparison with available experimental results and some numerical simulations tend to indicate that the proposed solutions may lead to a significant improvement compared with the original solution proposed by Mitchell et al., giving more realistic values for the factor of safety and required backfill strength [7].

Acknowledgments

The authors acknowledge the financial support of the Natural Sciences and Engineering Research Council (NSERC) of Canada and the partners of Research Institute on Mines and the Environment (RIME UQAT-Polytechnique; http://rime-irme.ca). Dr. R.J. Mitchell is gratefully acknowledged for his permission to use his published material.

References

[1] Benzaazoua M, Bussière B, Demers I, Aubertin M, Fried É, Blier A. Integrated mine tailings management by combining environmental desulphurization and cemented paste backfill: application to mine doyon. Miner Eng 2008;21:330–40.
[2] Hassani F, Archibald JF, Mine backfill (CD-ROM). CIM; 1998.
[3] Li L. A new concept of backfill design-application of wick drains in backfilled stopes. Int J Min Sci Technol 2013;23(5):763–70.
[4] Li J, Zhang J, Huang Y, Zhang Q, Xu J. An investigation of surface deformation after fully mechanized, solid back fill mining. Int J Min Sci Technol 2012;22(4):453–7.
[5] Zhang Q, Zhang J, Huang Y, Ju F. Backfilling technology and strata behaviors in fully mechanized coal mining working face. Int J Min Sci Technol 2012;22(2):151–7.
[6] Miao XX, Zhang JX, Feng MM. Waste-filling in fully-mechanized coal mining and its application. J China Univ Min Technol 2008;18(4):479–82.
[7] Mitchell RJ, Olsen RS, Smith JD. Model studies on cemented tailings used in mine backfill. Can Geotech J 1982;19:14–28.
[8] Zou DH, Nadarajah N. Optimizing backfill design for ground support and cost saving. In: Proceedings of the 41st US Symposium on Rock Mechanics. ARMA; 2006. p. 7–21.
[9] Dirige APE, McNearny RL, Thompson DS. The effect of stope inclination and wall rock roughness on back-fill free face stability. In: Rock engineering in difficult conditions: proceedings of the 3rd Canada-US rock mechanics symposium, Toronto; 2009. p. 9–15.
[10] Li L, Aubertin M. Numerical investigation of the stress state in inclined backfilled stopes. ASCE Int J Geomech 2009;9(2):52–62.
[11] Li L, Aubertin M. A modified solution to assess the required strength of exposed backfill in mine stopes. Can Geotech J 2012;49(8):994–1002.
[12] McCarthy DF. Essentials of soil mechanics and foundations: basic geotechnics. New Jersey: Prentice Hall; 2007.
[13] Bathurst RJ, Nernheim A, Allen T. Closure to 'Predicted loads in steel reinforced soil walls using the AASHTO simplified method' by Richard J. Bathurst, Axel Nernheim, and Tony M. Allen. ASCE J Geotech Geoenviron Eng 2011;137(12):1307–10.
[14] Bowles JE. Foundation analysis and design. McGraw-Hill; 1996.
[15] Becker DE, Moore ID. Canadian manual of foundation engineering. Canadian Geotechnical Society, Canada; 2006.
[16] Fall M, Nasir O. Mechanical behaviour of the interface between cemented tailings backfill and retaining structures under shear loads. Geotech Geol Eng 2010;28:779–90.
[17] Itasca. FLAC3D: Fast Lagrangian analysis of continua in 3 dimensions. Minneapolis: Itasca Consulting Group; 2006.
[18] Baxter CDP, Sharma MSR, Moran K, Vaziri H, Narayanasamy R. Use of $\bar{A}=0$ as a failure criterion for weakly cemented soils. J Geotech Geoenviron Eng 2011;137(2):161–70.
[19] Sariosseiri F, Muhunthan B. Effect of cement treatment on geotechnical properties of some Washington State soils. Eng Geol 2009;104:119–25.
[20] Sharma MSR, Baxter CDP, Moran K, Vaziri H, Narayanasamy R. Strength of weakly cemented sands from drained multistage triaxial tests. J Geotech Geoenviron Eng 2011;137(12):1202–10.
[21] Li L, Aubertin M. A three-dimensional analysis of the total and effective normal stresses in submerged backfilled stopes. Geotech Geol Eng 2009;27(4):559–69.
[22] Li L, Aubertin M, Belem T. Formulation of a three dimensional analytical solution to evaluate stress in backfilled vertical narrow openings. Can Geotech J 2005;42(6):1705–17.
[23] Li L, Aubertin M. An improved analytical solution to estimate the stress state in sub-vertical backfilled stopes. Can Geotech J 2008;45(10):1487–96.
[24] Li L, Aubertin M. An analytical solution for the nonlinear distribution of effective and total stresses in vertical backfilled stopes. Geomech Geoeng 2010;5(4):237–45.
[25] Li L, Aubertin M, Simon R, Bussière B, Belem T. Modeling arching effects in narrow backfilled stopes with FLAC. In: Proceedings of 3rd international symposium on FLAC and FLAC3D numerical modeling in geomechanics. A.A. Balkema 2003, p. 211–9.
[26] Li L, Aubertin M. A new solution for evaluating the required cohesion of a cemented backfill in underground stopes with an open face. Technical report EMP-RT-2013-07, École Polytechnique de Montréal.